



Experimentally Induced Thermal Fatigue on Lunar and Eucrite Meteorites—Influence of the Mineralogy on Rock Breakdown

Markus Patzek¹  and Ottaviano Rüsçh¹ 

¹Institut für Planetologie, Westfälische Wilhelms-Universität Münster, Münster, Germany



Key Points:

- We report on an updated experimental setup to simulate thermal fatigue in high vacuum instead of nitrogen atmosphere to reflect natural conditions
- The crack formation and growth rates differ between the lunar anorthosite and eucritic basalt and are generally <50% of those reported previously
- We propose that the resulting regolith depends highly on the mineralogy of starting materials, which control the breakdown of the rock

Supporting Information:

Supporting Information may be found in the online version of this article.

Correspondence to:

M. Patzek,
markus.patzek@uni-muenster.de

Citation:

Patzek, M., & Rüsçh, O. (2022). Experimentally induced thermal fatigue on lunar and eucrite meteorites— influence of the mineralogy on rock breakdown. *Journal of Geophysical Research: Planets*, 127, e2022JE007306. <https://doi.org/10.1029/2022JE007306>

Received 22 MAR 2022

Accepted 28 SEP 2022

Author Contributions:

Conceptualization: Markus Patzek, Ottaviano Rüsçh

Data curation: Markus Patzek

Formal analysis: Markus Patzek

Funding acquisition: Ottaviano Rüsçh

Investigation: Markus Patzek, Ottaviano Rüsçh

Methodology: Markus Patzek

Project Administration: Ottaviano Rüsçh

Resources: Markus Patzek

Supervision: Ottaviano Rüsçh

Validation: Markus Patzek

© 2022 The Authors.

This is an open access article under the terms of the [Creative Commons Attribution-NonCommercial License](https://creativecommons.org/licenses/by-nc/4.0/), which permits use, distribution and reproduction in any medium, provided the original work is properly cited and is not used for commercial purposes.

Abstract Thermal fatigue has been proven to be of fundamental importance for the nature and evolution of surfaces of airless bodies in the solar system. It is a rock erosive process acting in conjunction with meteoroid bombardment. We set up an experiment to simulate the diurnal temperature variation at 1 AU of centimeter sized sample cubes using a liquid nitrogen cooled cryostat, allowing to study unexplored conditions, that is, high vacuum and temperatures of 200 K similar to those occurring on the Moon. The sample cubes are investigated using scanning electron microscopy and micro computed tomography scans before and after 10, 20, 50, 100, and 400 total cycles. Cycling of the lunar anorthosite Northwest Africa (NWA) 11273 and the eucrite NWA 11050 reveal different behaviors: Whereas NWA 11273 responds to the cycling with micro-flaking of tenth-of- μm -sized grains on its surface and only limited crack growth, the eucrite NWA 11050 is less affected by micro-flaking but the growth of cracks is observed to occur throughout the whole experiment. The rate of crack formation and growth is lower when compared to previously reported results on ordinary and carbonaceous chondritic samples carried out under nitrogen atmosphere and above 250 K. We propose that the size of particles and their rate of production by thermal fatigue highly depends on the mineralogy of the exposed rock and areas with mature rocks are prone to produce fine-grained soil, while primary rocks such as basalts are likely to produce blocky regolith in a first step.

Plain Language Summary Thermal fatigue—the fatigue of a material due to temperature variation—is important for the breakdown of rocks on the surface of planetary bodies such as the Moon, asteroids, and also on the Earth and the formation of a fine-grained soil, called the regolith. With an improved experimental setup, we simulate the diurnal temperature variations at a solar distance of 1 AU under high vacuum conditions between 200 and 375 K for the lunar anorthosite breccia Northwest Africa (NWA) 11273 and the eucritic basalt NWA 11050. We show that both types of rocks respond different to these temperature excursions: The basaltic eucrite forms cracks over the course of 400 cycles and the lunar anorthosite tends to flake off tenth-of- μm -sized grains with only limited cracking. The overall obtained cracking rates are lower when compared to those from previous experiments under nitrogen atmosphere, indicating the retrieved breakdown rates are lower than previously reported and the type of resulting soil depends strongly on the mineralogy of the exposed rock.

1. Introduction

Airless planetary bodies exhibit conditions that modify material on the surface in different ways: micrometeorite and meteorite impacts and following impact brecciation (e.g., Bischoff et al., 2006, 2018; Cambioni et al., 2021; Horz & Cintala, 1997; Keil, 1982; Pieters & Noble, 2016; Stöffler et al., 1988), diurnal temperature variations due to the rotation of the planetary body (e.g., Delbo et al., 2014; Molaro et al., 2015), and constant bombardment by protons (e.g., Barghouty et al., 2011; Housley et al., 1974) degrade the material on the surface in a variety of fashion and on different spatial and temporal scales. Understanding these modification processes is key in understanding the evolution of planetary surfaces and the preservation of material that might be embedded near the surface, such as organics and ices.

While the effect of micrometeorites (<~1 mm) and protons mainly affect the uppermost layer (micrometer scale) of the planetary bodies, larger meteorite (>>~1 mm) impacts are able to excavate fresh material from deeper layers and expose it to space. Diurnal temperature variations will develop different types of stresses (e.g., Ravaji et al., 2019): Stresses driven by mineral heterogeneities and temperature gradients are below the material yield strength and leads to sub-critical crack growth, that is, a fatigue process, whereas stresses driven

Visualization: Markus Patzek
Writing – original draft: Markus Patzek
Writing – review & editing: Ottaviano Rüsch

by spatiotemporal temperature gradients can exceed the material yield strength and leads to super-critical crack growth, that is, a shock process (e.g., Molaro et al., 2015, 2017). In principle, these stresses can occur both at the grain-and boulder-scale (e.g., Molaro et al., 2015, 2017). The magnitude of the stress field inducing sub-critical crack growth is mainly controlled by the amplitude of the temperature differences during day and night. The fractures resulting from these stresses likely lead to rock breakdown and should eventually turn a fresh, blocky surface continuously into a fine regolith.

Several recent advances regarding thermal fatigue focused on asteroids and, specifically, on the effect of the rock size subject to diurnal temperature variations (Ravaji et al., 2019), the effect of very high rate of temperature change (Libourel et al., 2021), crack propagation direction (Uribe-Suárez et al., 2021), and exfoliation and particle ejection on asteroids (Molaro, Walsh, et al., 2020). The current understanding of thermal fatigue in breaking down rock on the Moon, instead, is limited (Molaro et al., 2015, 2017; Ruesch et al., 2020) and thus prevent a reliable understanding of its surface evolution (Hörz et al., 2020). In this study we address two major aspects of thermal fatigue on planetary material that have remained largely unexplored. The environment effects (vacuum, representative minimum temperatures) and the effect of lunar petrology. The past experimental studies investigating the effects of thermal fatigue on rock breakdown have been carried out in atmosphere accepting several problems including, as detailed further below, enhanced thermal conductivity, the reduction of surface energy by the adsorption of water molecules onto grain surfaces leading to enhanced crack propagation rates (Atkinson, 1984; Krokosky & Husak, 1968; Orowan, 1944), and minimum temperatures well above the actual minimum reached during night on planetary bodes.

This work describes an improved experimental setup taking these problems into account by using an evacuated cryostat making it also possible to simulate temperatures as low as 200 K and even below that. In order to investigate the effect that thermal cycling has on lunar rocks, whose petrology is dramatically different from that of asteroids, two samples are chosen to represent the lunar highland material and the lunar mare.

2. Previous Experimental Studies on Diurnal Temperature Variations

A first attempt to characterize the effect of thermal fatigue due to diurnal temperature variation on meteorites was presented in Levi (1976). In that study H chondrite samples were cycled between 83 and 373 K for several hundred times, each cycle with a duration of 53 min. Thermal fatigue effects were reported to be fracturing of sulfides, cleavage, undulatory, and anomalous extinction: in general features similar to those ascribed to shock or static loading. Samples were immersed in liquid nitrogen protected by several layers of aluminum to avoid thermal shock. In our opinion, however, it is not clear whether such procedure really avoided thermal shock. If it occurred, the very high thermal gradient would be unrealistic for airless planetary surfaces around 1 AU and would explain the important changes observed.

More recently, the study of Delbo et al. (2014) used a climatic chamber to conduct thermal cycling between 250 and 440 K, for 407 times and with 2.2 hr per cycle. The carbonaceous chondrite Murchison (CM; Mighei-like) and the ordinary chondrite (OC) Sahara 97210 (L/LL3.2, S4) were selected. Using non-destructive micro-computed tomography scans (μ -CT), the growth of fracture length and volume were recorded as a function of increasing cycle numbers. These measurements were coupled to a micromechanical model of meteorites in order to extrapolate the cracks development until final rock fragmentation. Importantly, for the specific case of Near Earth Asteroids (NEA), the fragmentation rate due to thermal fatigue was found to be higher than that due to meteoroid bombardment. Later, Molaro et al. (2017) performed simulations using similar parameters and they showed, that the calculations carried out by Delbo et al. (2014) are overestimating the break down rates due to an inaccurate application of the Paris law on their initial crack size. Open questions left by this study are the following:

1. What is the effect of reaching the low temperatures experienced on asteroids and the Moon (\sim 200 K) considering that at such temperatures ($<$ 250 K) meteorites have anomalous thermal expansion (Opeil et al., 2020). Thermal expansion coefficient is a key property controlling grain-scale thermal fatigue (Molaro et al., 2015).
2. What is the effect of high vacuum on thermal fatigue considering that (a) adsorbed water molecules decrease the surface energy and the tensile strength (e.g., Orowan, 1944) and thus enhance crack propagation (e.g., Eppes & Keanini, 2017); and (b) gases around and within porous meteorites convect heat and might affect spatial as well as temporal thermal gradients, which otherwise occurs by conduction and is primarily controlled by the abundance of cement between grains (Piqueux & Christensen, 2009)? The study

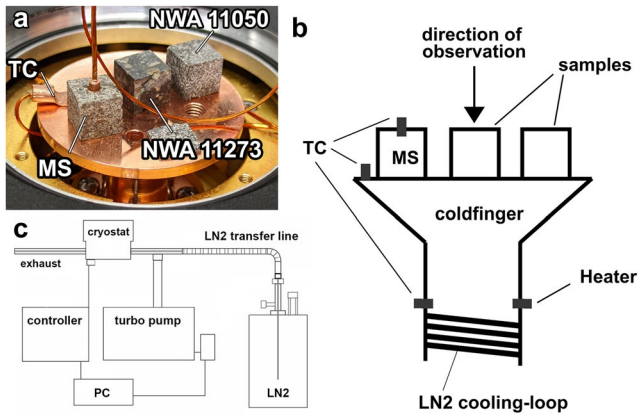


Figure 1. (a) Close-up photograph of the custom-made cold finger with attached thermocouple (TC), monitor sample (MS) El Hammami (H5) and studied cubes of eucrite NWA 11050 and the lunar anorthosite NWA 11273. For completeness, the flat gray sample is a test sample for infrared thermometry not considered in this work. (b) Detailed sideview of the Cu-cold finger as well as heating and viewing geometry. The LN₂ cooling loop on the base of the cold finger is constantly cooled and the heater located close to it is able to provide enough energy to heat the cold finger to temperatures of 375 K. The different thermocouples (TC) are used to monitor the temperatures at different locations of the cold finger (i.e., base close to the heater, cold finger-top, and MS). The samples resting on the cold finger are therefore heated/cooled from the bottom and viewed from the top, that is, opposite side, protecting the surface from mechanical contact such as handling. (c) Schematic view of the whole experimental setup built around the cryostat. A predefined temperature profile is defined and transferred to the controller, which maintains the correct energy input into the system to fulfill the preset temperature profile. See text for additional details.

of Delbo et al. (2014) performed cycling in nitrogen atmosphere with samples previously exposed to a vacuum of 1×10^{-2} bar before cycling. As mentioned in Molaro et al. (2017), it is not known whether these precautionary steps eliminated moisture from the samples. Additionally, it may well be possible, N can affect the crack formation in similar ways as water molecules, although in a lesser extent. Most artificially caused outgassing from samples in vacuum stops after seven cycles at about 4×10^{-6} mbar, suggesting that their samples likely had moisture (Figure S3 in Supporting Information S1).

3. What is the possible effect of terrestrial weathering on the selected meteorite samples prior to experimentation, considering its impact on physical parameters? Oxidation of metal can weaken the rock by its volume increase if the primary porosity is low or the abundance of metal is high (e.g., Lee & Bland, 2004)? Additionally, iron hydroxide may act as a cement filling primary porosity and change the thermal conductivity of the sample. The actual degree of weathering and its influence on the rock have been proven absent for the sample in this study, from which the cubes have been prepared. A thin section of Sahara 97210 used in the study of Delbo et al. (2014) has visible effects of terrestrial alteration as proven in thin sections available in the Institut für Planetologie meteorite collection (Text S2, Figure S2 in Supporting Information S1).
4. More generally, how do other meteorite types of drastically different petrology respond to thermal fatigue near conditions at 1 AU with a temporal thermal gradient of about 2 K/min?

The most recent study of Libourel et al. (2021) has shed light on the spatial properties of cracks for three different type of meteorites: the ordinary chondrite Sahara 97210, the Vigarano-type (CV3) meteorite Allende, and the CM chondrite Murchison. It is to be noted that the thermal cycling performed in Libourel et al. (2021) was carried out with a high temporal and spatial thermal gradient and high temperatures (up to 713 K), specifically designed to investigate the conditions experienced by low perihelion asteroids, and not representative for the thermal conditions at 1 AU.

Nevertheless, fractures observed with scanning electron microscope (SEM) were reported to be drastically different for different meteorites type with widths of 40–50 μm in Murchison, 5–10 μm in Allende and <5 μm in Sahara 97210. A network of fractures developed in all samples, although with different level of branching for the different samples (Figure 9 in Libourel et al., 2021). Contrary to previous experimental findings (Hazeli et al., 2018; Liang et al., 2020) and theoretical modeling (e.g., Molaro et al., 2015), fractures were observed to develop around, as well as through, chondrules. The study of Liang et al. (2020) investigated the 3-dimensional distribution of stresses on a L6 ordinary chondrite due to thermal loading and determined that stress concentrates along the matrix-particle interface, supporting previous findings in 2-dimensions (Hazeli et al., 2018). Instead, from the most recent study of Libourel et al. (2021), it seems that fracture propagation at the matrix-particle interface is not representative of the development of an entire fracture network developed under thermal fatigue. Thus, despite these findings, the details of where fractures form and propagate with respect to different meteoritic components (i.e., chondrules, matrix, metal, and sulfides) are not known. However, the high thermal gradient used by Libourel et al. (2021) is very likely acting in a thermal shock regime instead of thermal fatigue rendering it difficult to compare different experiments.

3. Experimental Setup, Methods, and Samples

3.1. Setup

From the review of literature above and the raised questions, the requirements for the sample selection and experimental setup are the following. (a) Samples need to be free from terrestrial weathering, (b) samples need to be placed in high vacuum ($<1 \times 10^{-5}$ mbar), and (c) a cryogenic cooling system is needed to reach low temperatures. These requirements are met by developing an experiment around a cryostat evacuated to pressures in the range of 1×10^{-5} – 1×10^{-6} mbar (Figure 1), which is dramatically different to previous studies that work under

1×10^3 mbar. Sample cubes are placed in the cryostat and degassed for at least 48 hr at the maximum temperature of the planned experiment (~ 375 K), which roughly equals the time of stable liquid nitrogen flow required for reproducible cycles. Inside the chamber, a radiation shield of Au-coated Cu plates is shielding the interior part of the cryostat from radiation warming due to the temperature of the casing. On the base of the liquid nitrogen heat exchanger, a Si diode temperature sensor is located. Additionally, a 100 W resistance heater is located close to the heat exchanger to allow for temperature increase. Through an additional port, connectors for type K thermocouples are installed to measure the temperature on the surface of the cold finger and on the monitor sample. The monitor sample is a 1 cm^3 cube of the H5 chondrite El Hammami to which the thermocouple is attached to and that is used to monitor the temperature of the sample cubes. The temperature difference between monitor sample and the cold finger surface is maximum 2 K proving that the thermal conductivity between cold finger and sample is guaranteed. The Si diode, the resistance heater, and the three thermocouples are connected to a Model 336 Cryogenic Temperature Controller manufactured by Lake Shore company. By using this temperature controller, automatic heating curves and variable input sensor can be set to allow automatic and reproducible temperature change. Experimental files for the experiments can be loaded conveniently and be fully and automatically controlled by a script.

The minimum and maximum temperatures were selected to be 200 and 375 K, respectively: these are typical values reached by the outermost parts of lunar rocks (Bandfield et al., 2011; Molaro et al., 2017). The temporal temperature gradient (dT/dt) was kept as low as possible to be similar to the lunar rock conditions, while still enabling the experiment to be run in a practically reasonable time. Temperature gradient of the samples was set at 1.8 K/min and was kept constant throughout the cycling. No measurement of dT/dt of lunar rocks measured in situ exists. Modeling of the temporal gradient indicate values between 0.4 and 1.0 K/min, depending on rock albedo, emissivity, density, heat capacity, thermal conductivity, as well as geometric and temporal conditions (Molaro & Byrne, 2012). Since several of these properties are not well known, the 1.8 K/min rate can be considered a realistic value, albeit it likely represents an upper limit. In this respect, the present experiment should be considered one favoring the effects of thermal fatigue, although defining the thermal regime and the expected stress fields is hard to determine due to the complex nature of the samples (see Section 3.4 for further details on the thermal gradients and regimes). The sample cubes are placed on the cold finger on the exact same side for experimental step.

3.2. Methods

Crack development is studied by observing the samples at the following intervals between thermal cycling: 0, 10, 20, 50, 100, and 400 cycles. A higher observation rate at the beginning is motivated by findings of early crack development by Delbo et al. (2014). For observation of the top surface (i.e., the opposite side of heating) of the sample cubes, a JEOL 6610-LV SEM is used and operated at 20 kV acceleration voltage with 1.5 nA probe current at a magnification of 200x in low-vacuum mode at a pressure of 0.4 mbar in backscattered electron mode. The images are processed into a mosaic resulting in a pixel resolution of approximately 330 nm per pixel, although slight differences in the sample height lead to focus gradients resulting in an effective resolution of 1 μm per pixel. The SEM-BSE images are gray-scale images, where brighter areas are composed of minerals with higher density, that is, more heavy elements. Metallic iron, would be therefore bright, and pure SiO_2 very dark. After each run, a SEM-BSE map is obtained before investigation by micro-computed tomography scans ($\mu\text{-CT}$).

Obtained SEM-BSE maps are then transferred to ESRI ArcGIS software and referenced to each other allowing to compare the different runs and determine changes on the surface. Different types of features were categorized and measured using the pixel resolution of 1 px \approx 3 μm .

3D $\mu\text{-CT}$ scans of the sample cubes were obtained after each run using a Zeiss Xradia 520 Versa operated at 80 kV resulting in a voxel (3D pixel) size of approximately 15 μm . After recombination, the cubes for each run were aligned using the software Dragonfly from Zeiss and the built-in images registration.

3.3. Samples

Since the experimental configurations are set up to constrain the conditions for the Moon, we selected samples that are representative of the lunar surface, that is, basaltic rocks (mare basalts) and consolidated anorthosite breccias (highlands). Photographs of the samples prior to the experimental procedure are shown in Figure 2.

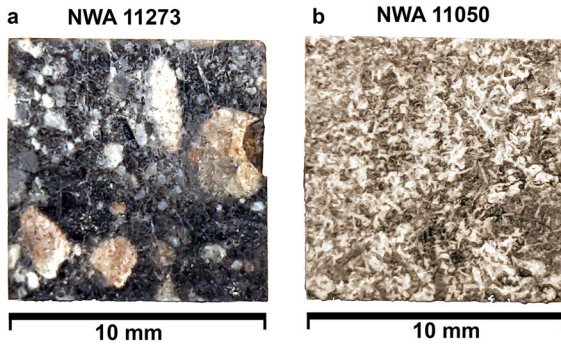


Figure 2. Photograph of the samples taken in optical light before experiments. (a) Lunar anorthosite breccia NWA 11273 with visible mineral and rock fragments (white and brown, respectively) embedded into a dark fine-grained, often glassy matrix. (b) Eucrite NWA 11050 displaying a typical basaltic texture with euhedral, lath-shaped pyroxene crystals (white) embedded into a dark matrix of xenomorphic plagioclase-dominated groundmass. Accessory minerals cannot be identified in these images.

Northwest Africa (NWA) 11050 is a monomict eucritic breccia. This eucritic sample likely formed on a large basaltic asteroid, likely (4) Vesta (e.g., Righter & Drake, 1997). Since its texture, mineralogy, and major elements are very similar to basaltic rocks formed on the Moon, this sample can be considered representative of typical lunar basaltic rocks found on the mare regions. The sample consists of lithic clasts with ophitic to subophitic textures set in a fine-grained clastic matrix of eucritic debris (Figure 3a). Pyroxene crystals ($\text{Fs}_{57}\text{Wo}_{29}$) of varying sizes exhibit thin exsolution lamellae of augite ($\text{Fs}_{27}\text{Wo}_{41}$). Melt pockets consisting of a silica polymorph, ilmenite, and troilite are frequently found within lithic clasts. Plagioclase grains of variable sizes range in composition from $\text{An}_{80}\text{Or}_0$ to $\text{An}_{99}\text{Or}_2$. Metal is rare and the effects of terrestrial alteration are limited to edges of metal grains in the here studied sample. A representative SEM-BSE image showing the petrologic context of the sample is shown in Figure 1a. A $10 \times 10 \times 10 \text{ mm}^3$ cube was prepared from a fusion crust-free area of eucrite NWA 11050 by sawing the rough shape and gradually polishing in ethanol on a 400-grit polishing plate without the use of epoxy to remove excess relief and damaged material, and visually inspected for any uncommon mineralogical or physical features (large voids, large single minerals, etc.). One side was chosen for

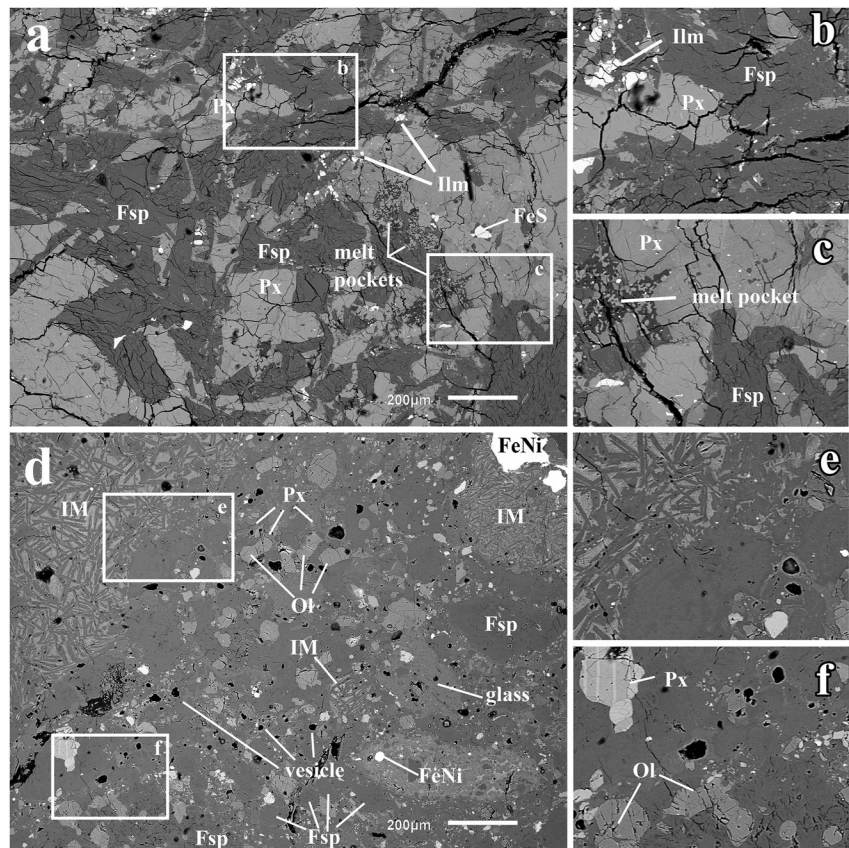


Figure 3. (a) Scanning electron microscope (SEM)-backscattered electron mode (BSE) image of a typical area in the monomict eucrite NWA 11050 with pyroxene (Px) and plagioclase (Fsp) crystals as their main constituents. Occasionally, ilmenite (Ilm) and troilite (FeS) can be found. Melt pockets with SiO_2 phases are also abundant in this sample. Close ups of two areas are shown in b and c, respectively. (d) SEM-BSE image of a typical area in the lunar anorthosite breccia NWA 11273 with clasts of impact melt (IM), olivine, pyroxene of different composition (and therefore different brightness) and anorthite in a fine-grained matrix that commonly has vesicles (here black). Close ups of two areas are shown in e and f, respectively. Both images are obtained on polished thin sections of the samples from which the cubes were prepared.

continuous observation using SEM-BSE imaging in low-vacuum mode (see methods) to track changes over the course of thermal cycling.

NWA 11273 is a lunar anorthosite breccia composed of mineral and lithic clasts of anorthite, olivine, pigeonite, augite, chromite, Ti-Cr-Fe spinel, kamacite, rare taenite, and abundant troilite in a fine-grained matrix commonly having vesicles of different sizes. Impact metal fragments are commonly observed. Barite grains are sometimes identified and rare basalt clasts and glass fragments are also present. A representative SEM-BSE image showing the petrologic context of the sample is shown in Figure 3d. Based on the bulk FeO and Th concentration, Zeng et al. (2020) proposed a launch region of anorthosite breccia NWA 11273 to be in the anorthositic-Feldspathic Highland Terrane (FHT-An) and to regolith around the FHT-An in the outer-Feldspathic Highland Terrane. Similar to the eucrite NWA 11050, a $10 \times 10 \times 10$ mm³ cube was prepared from a fusion crust-free sample, inspected from all sides and finally one side chosen for the continuous observation.

3.4. Thermal Fatigue Versus Thermal Shock

For the thermal cycling in this experiment, about 2 K/min was chosen as a heating and cooling rate. This rate was primarily chosen due to the expected rates on surfaces of planetary surfaces located at ~1 AU with rotation rates similar to the Moon and because of its similarity to previously used rates and the most comparable study carried out by Delbo et al. (2014).

However, several studies suggested that a rate of 2 K/min is the requirement and at the same time a guarantee to experience thermal fatigue below this threshold and thermal shock above it. The 2 K/min temporal gradient has first been evoked in Richter and Simmons (1974) and was based on measured thermal expansion coefficients of terrestrial basalts. That study concluded that crack propagation due to macroscopic spatial temperature gradients and crack propagation along grain boundaries due to differences in thermal expansion coefficients of the minerals occur in different thermal regimes; the 2 K/min value was established as a threshold to distinguish between the two regimes. This is, however, too generalized and not necessarily correct to predict damage due to thermal stresses. Nonetheless, this threshold self-propagated throughout the literature and is an oft-used criteria to determine the thermal regime an experiment is acting in Boelhouwers & Jonsson (2013); Molaro et al. (2015). As shown by Molaro et al. (2017), determining the magnitude of stress a sample (boulder) experiences under certain conditions is difficult, since these natural samples are usually complex aggregates of different minerals, constituents, and pre-existing weaknesses resulting in complex stress fields. The sample size selected in this study is certainly smaller than the thermal skin depth for lunar rocks modeled in Molaro et al. (2017), likely excluding substantive bulk stresses to develop. Based on this, the applied experimental setup is likely resulting in the formation of stress fields and ultimately cracks due to heterogeneities in the microstructure of the rocks. The shape and effect of the stress fields developing in different samples is highly dependent on the experimental setup and environment (e.g., Molaro et al., 2017). Changing the temporal heating and/or cooling gradients might affect the shape and extent of the stress field developing in a sample or boulder. Thus, arguing whether this experiment is solely acting in thermal fatigue or thermal shock regime is impossible without modeling the exact internal structure of the samples. However, the selected sample size with respect to the thermal skin depth for lunar conditions and the selected temporal temperature gradients with regard to previous studies and the expected gradients on the Moon render it likely that the experimental conditions favor thermal fatigue over thermal shock.

4. Results

Investigating the SEM-BSE images of the top surface (i.e., opposite side of heating) revealed different types of changes on the sample surfaces: (a) flakes that move from observation to observation and eventually get lost or relocated; (b) larger multi grain aggregates that move or rotate; and (c) cracks forming and increasing their length and width. While type a and c changes are commonly observed, grain rotation (b) is rarely observed on both samples preventing us from drawing any conclusions on them. Examples of flakes are shown in Figure 4.

The lunar anorthosite breccia NWA 11273 and the eucrite NWA 11050 differ in their response to the thermal cycling experiment as will be described in detail below. Cracks observable in SEM-BSE images developed on both samples, however, their size never reached the resolution of the μ CT scans carried out (voxel size of ~15 μ m) and therefore details on the 3D data are not discussed.

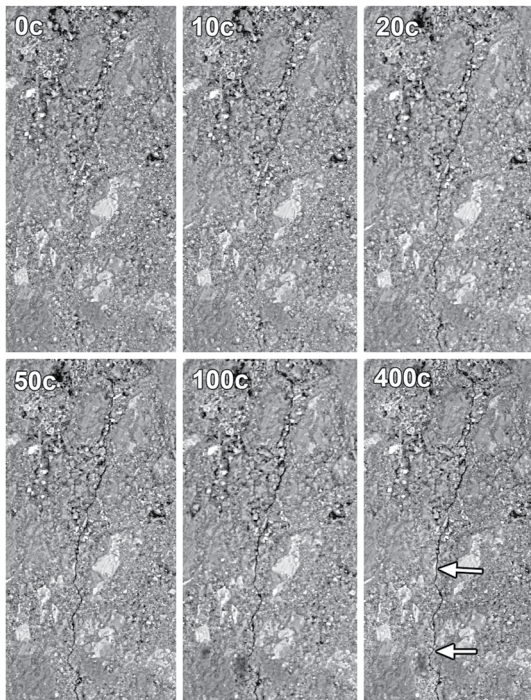


Figure 4. Typical surface changes observed for lunar anorthosite breccia NWA 11273 are particles that are produced by surface-near cracks. These particles are likely to be spalled away during further cycling and scanning electron microscope observation. For clarity, the arrows point to the location, where flaking is observed. The numbers refer to the total cycles ran for this image. (a–d) show two locations after 50 and 30 additional cycles, respectively. From (a to b) a flake is disappearing (see arrows). (c–d) Show a different location, where a small part of a grain is disappearing (see arrows). (e–h) Show the evolution of a micro-flake on a different location by cracking of the surface after 100 total cycles (see arrows). After 400c the micro-flake was spalled off from the surface. Image width is $\sim 100 \mu\text{m}$ for all panels.

4.1. Lunar Anorthosite Breccia NWA 11273

Flakes: Investigation of the SEM-BSE mosaic of the lunar anorthosite breccia NWA 11273 after 10, 20, 50, 100, and 400 total cycles revealed 101 flakes with sizes ranging from ~ 6 to $\sim 46 \mu\text{m}$ (Figure 5a). Most of these flakes are part of the sample before, whereas other appear to be rather loose before (see discussion). Flake occurrence is not limited to a specific silicate mineralogy within the sample, that is, appears on glass fragments, in matrix areas as well as on anorthite and olivine grains, but is not observable on metal or sulfide. Some flake occurrences are shown in Figure 4 showing three different locations, where micro-flaking is happening at different numbers of cycles (a + b, c + d, and e + f + g + h). 80% of the micro-flaking occurrences are observed after 50 and more cycles, resulting in only $\sim 20\%$ happening in the first 20 cycles (Figure 5b). Assuming a micro-flake thickness of $3 \mu\text{m}$, the lost volume per cycle (rotation period) on a 100mm^2 area is $2 \times 10^{-6} \text{mm}^3$.

Cracks: A total of 27 crack formations and/or extensions could be detected after 400 cycles on lunar anorthosite NWA 11273. Most of these cracks (24 out of 27) create micro-flakes and lead to their detachment (Figures 4e–4h), basically probing the ongoing flaking process that is acting in the uppermost surface. While no crack is visible in the untreated sample (Figure 4e, 0c) and after 50 initially cycles (Figure 4f, 50c), a crack developed after 100 total cycles (Figure 4g) leading to the formation of a flake, which detached after 400 total cycles (Figure 4h). The remaining three cracks (3 out of 27) are obviously penetrating deeper into the sample or, alternatively have not let to flaking yet, since we are not able to detect them in the interior of the sample.

4.2. Eucrite NWA 11050

Flakes: Flakes of various size have been observed to move around or get lost on the surface of eucrite NWA 11050. In total, 17 flakes were determined after a total of 400 cycles (Figure 5). There is no indication that these flakes are limited to a specific mineralogy within the sample, although this could be attributed to the low absolute number of micro-flaking detected on this sample preventing reliable statistics.

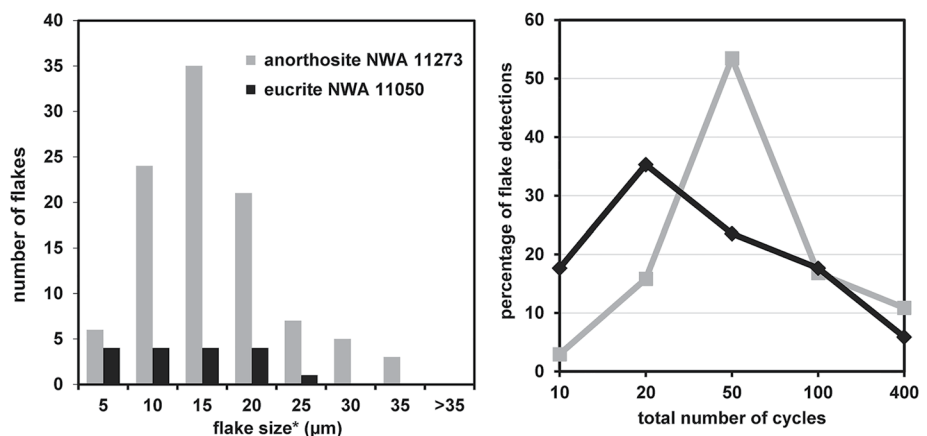


Figure 5. (a) Histogram of micro-flaking occurrences and their size in μm for the lunar anorthosite breccia NWA 11273 (gray) and the eucrite NWA 11050 (black). *Calculated (square-root) flake size assuming squared flakes for visualization, since their size was measured as polygons. (b) Percentage of flake formation relative to the total number of cycles ran. For example, 50% of all micro-flakes on anorthosite breccia NWA 11273 were detected after 50 total cycles.

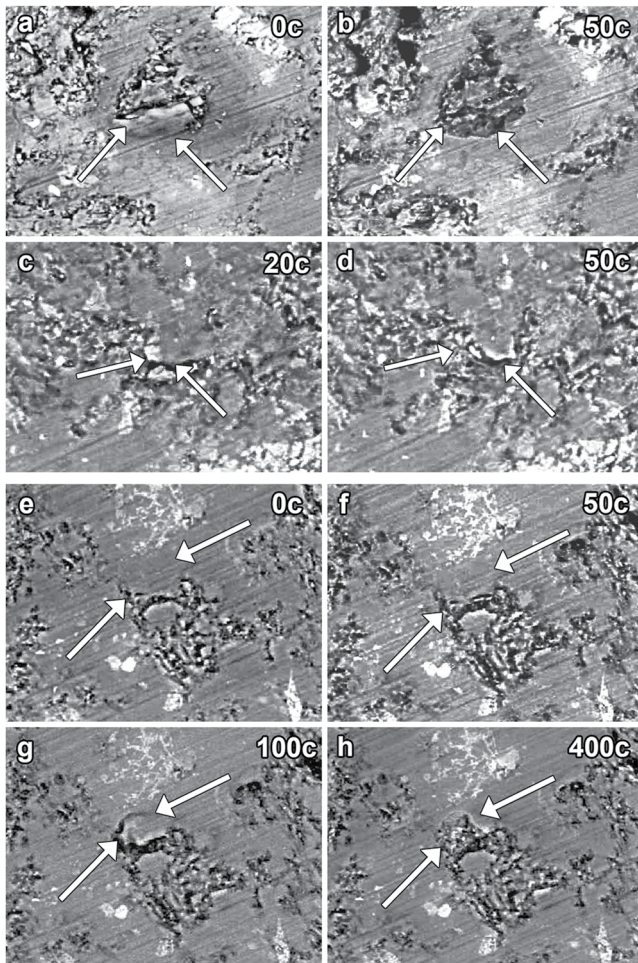


Figure 6. Area of the top surface of eucrite NWA 11050 eucrite showing a crack that successively opens up to a maximum of $\sim 5 \mu\text{m}$. Image width is $\sim 200 \mu\text{m}$. The crack was already slightly visible in the untreated sample (0c), but clearly widens up after 20 cycles and extends downward in the image orientation. The crack length increased further over the course of 50c–400c, which is not shown here for visualization purpose, although its width is constantly increasing at various locations (see arrows).

Cracks: The formation and extension of cracks on the surface of eucrite NWA 11050 can be observed after already 20 cycles (e.g., Figure 6). In total, 41 cracks were detected on the samples with lengths ranging from ~ 5 to $\sim 636 \mu\text{m}$. The length and width have been observed to increase with an increasing number of cycles for some of the cracks. However, the width change is usually on the order of a few pixel only and close to the detection limit set by the method. Therefore, the crack width of the newly formed and extended cracks is well below the resolution of the $\mu\text{-CT}$ scans ($\sim 15 \mu\text{m}$ voxel size). A majority of the cracks are forming and extending along grain-grain boundaries or in brecciated, fine-grained, areas between different lithologies, and mineral fragments, that is, between anorthite and pyroxene ($\sim 60\%$), in polycrystalline anorthite-dominated areas ($\sim 15\%$), and brecciated fine-grained cataclastic areas (20%). Only $< 5\%$ of the cracks develop in pyroxene grains.

5. Implications

5.1. Micro-Flaking on the Surface of Rocks

Micro-flaking on the surface is $\sim 5\times$ more abundant on the lunar anorthosite, when compared to that of the eucrite sample (Figure 5a). This difference in micro-flaking abundance is likely due to the strong mineralogical difference between the two samples. Micro-flaking is observed often on plagioclase and glassy areas, although it is noteworthy, that the lunar anorthosite is mainly composed of anorthite and brecciated glassy melt pockets indicating micro-flaking occurrences on these components will likely dominate over that on other components (compare Figure 3a). During transport, and also during electron bombardment at the SEM, electrostatic charging might be able to dislocate small flakes. This leads to the question of whether handling and preparation of the samples introduced artificial damage to the samples that is favoring micro-flaking. For the preparation of the samples, we relied on the standard procedure carried out for sample preparation in meteoritics and geology established for several decades. This includes initial sawing of rocks followed by gradually finer polishing to remove the damaged layers and end up with a smooth and intact surface. The general procedure and the forces acting on the sample are tremendously different from those being applied during for example, grinding rocks in mining processes (e.g., Liu et al., 2019), as well as sawing and polishing (e.g., Jiang et al., 2020). There are additional arguments supporting the thermal stress induced micro-flaking: First, we note that the force applied on the samples during, for

example, sawing and polishing is less than during bedrock fragmentation by impact cratering, that is, the primary mechanism of formation of lunar rocks. Second, sawing and polishing is a well-established process for sample preparation of meteorite and geologic samples proven suitable for maintaining internal microstructures of crystals. Third, since both samples are prepared and handled the exact same way (see Section 3), the observation that the lunar anorthosite tends to micro-flaking indicate that its mineralogy is prone to produce small tenth-of- μm -sized flakes. Fourth, the observation that only $\sim 20\%$ of the observed micro-flaking happened after the first 20 cycles and therefore the vast majority after this (Figure 5b), indicates that most of the micro-flaking is not a preparation artifact but a result of the cycling since artificial damage would lead to micro-flaking in the beginning of the experiment rather than in the end. Fifth, as presented in the results, 23 out of 27 cracks detected on lunar anorthosite breccia NWA 11273 surface lead to micro-flaking probing the ongoing flaking process and indicating that the thermal cycling is causing this. However, the uncertain contribution by sample handling allows only for an uppermost estimate of the eroded volume by micro-flaking. Since micro-flaking was less often observed on the eucrite, the statistics for this sample may not be robust enough to speak for or against an artifact (Figure 5a). This micro-flaking is a relevant process for the formation of fine-grained particulate material on the surface of the Moon. Already in the 70s, Carrier (1973) have studied the nature of lunar soil and concluded that the median

particle size is 40–130 μm with an average of approximately 70 μm . Taylor et al. (2010) studied lunar highland soils collected during Apollo 14 and 16 with respect to their grain size and composition. They stated that for the 10–20 μm size fraction of anorthositic Apollo 16 soils with higher glass abundances, the plagioclase abundance will be increased relative to the “mafic silicates fraction.” This bears important implications for remote sensing and especially for reflectance measurements, since these measurements are dominated by the 10–20 μm fraction (e.g., Warren & Korotev, 2022). The observed micro-flaking on lunar anorthosite breccia NWA 11273 is acting on exactly this grain size fraction (Figures 3 and 4a), and since its mineralogy is dominated by plagioclase and glass (Figure 3a), it is possibly one reason for the observed characteristics of Apollo 16 soils. Additionally, the easy cleavage of feldspars such as plagioclase can act in favor for producing small particles of this mineral (e.g., Klein et al., 1985). The easier comminution of feldspar relative to for example, pyroxene or olivine has also been proven to be more effective with respect to impact experiments (Cintala & Hoerz, 1992; Hörz et al., 1984, 2020).

This, however, may only be applied to the regions where rocks similar to lunar anorthositic breccias are available, likely the highlands outside the South Pole-Aitken basin (Zeng et al., 2020). Hörz et al. (2020) reported on the influence of micrometeorite impacts on the alteration of lunar surface rocks. Especially micrometeorite impacts produce weak spots on the surface in spallation zones, that are prone to removal since they undercut the pit and only require little energy to be removed (Hartung et al., 1972; Hörz et al., 1971, 2020). These spallation zones might lead to preferred micro-flaking around the $\sim > 10 \mu\text{m}$ impact pits.

Assuming that the observed micro-flaking continues at constant rates over long period of times, an abrasion rate can be estimated, albeit only on an order of magnitude basis due to the unknown role of saw cut damages during sample preparation (e.g., Liu et al., 2019). The order of magnitude of the abrasion rate can be estimated to be 1×10^{-2} mm/Myr for rock surface on the Moon of the same composition as NWA 11273. Since we consider that the observed eroded volume of micro-flaking is the maximum possible value, and that the temporal thermal gradient in the experiment is at the upper end of the likely range experienced by actual lunar rocks, thus eventually favoring thermal fatigue, this rate of erosion by micro-flaking is an upper estimate. This rate is an order of magnitude lower than the average value of abrasion associated to micrometeoroid bombardment (Croaz et al., 1971). However, in some studies, values for micrometeoroid abrasion similar to the rate estimated here have been reported (Hörz et al., 1974; Shoemaker, 1971). Therefore, we cannot exclude that for rocks of specific petrology, abrasion could be dominated by micro-flaking rather than micro-meteoroid bombardment. As remarked by MacLennan & Emery, 2022, a regolith formation solely by accumulating fine-grained soil due to the breakdown by thermal fatigue will essentially come to halt after a certain soil thickness is accumulated that exceeds the thermal skin depth. In any case, on the Moon, catastrophic shattering of any rock size and type will occur by meteoroid impact at a rate higher than by abrasion (Hörz et al., 1974) allowing constant formation of micro-flakes.

Molaro, Walsh et al. (2020) state that boulder exfoliation observed widely at Bennu is likely to be driven by near-surface stresses due to thermal fatigue. Additionally, Molaro, Hergenrother et al. (2020) argue that these exfoliations are likely causing the ejection of particles from Bennu's surface into space, which has been commonly observed. Exfoliation is suggested to be the consequence of separation after micro fracture coalescence into large fractures (Molaro, Hergenrother et al., 2020), and we propose that the micro-flaking observed in this experiment is the small-scale counterpart to the cm-to m-scale exfoliations observed on Bennu. However, since the geometry of heat influx and therefore the shape and orientation of stress fields in the samples and on Bennu's boulders is different, modeling of these stress fields is essentially needed in future.

The here studied eucrite NWA 11050 is less affected by micro-flaking relative to the lunar anorthosite breccia NWA 11273 (Figure 5a) indicating its mineralogy and structure is not as “friable” to this process as the lunar anorthosite. Since the eucrite (although it is also a breccia) is closer to a primary rock in its maturity with an assemblage of primary minerals that formed from a lava flow rather than a mature breccia containing glassy matrix implies that reworked, but consolidated, rocks such as those found on the lunar highlands are prone to produce a fine-grained soil by micro-flaking. Rocks with a primary mineralogy (i.e., volcanic or possibly metamorphic) are prone to be fractured by cracks due to diurnal temperature variations. We thus propose that surfaces exposing solid primary rocks are less likely producing fine-grained soil by thermal fatigue but rather produce larger fragmented (blocky) regolith, with fragments produced by cracks extending through the source rock (Figures 6 and 7). On the other hand, mature regolithic rocks such as the lunar anorthosite breccias and those

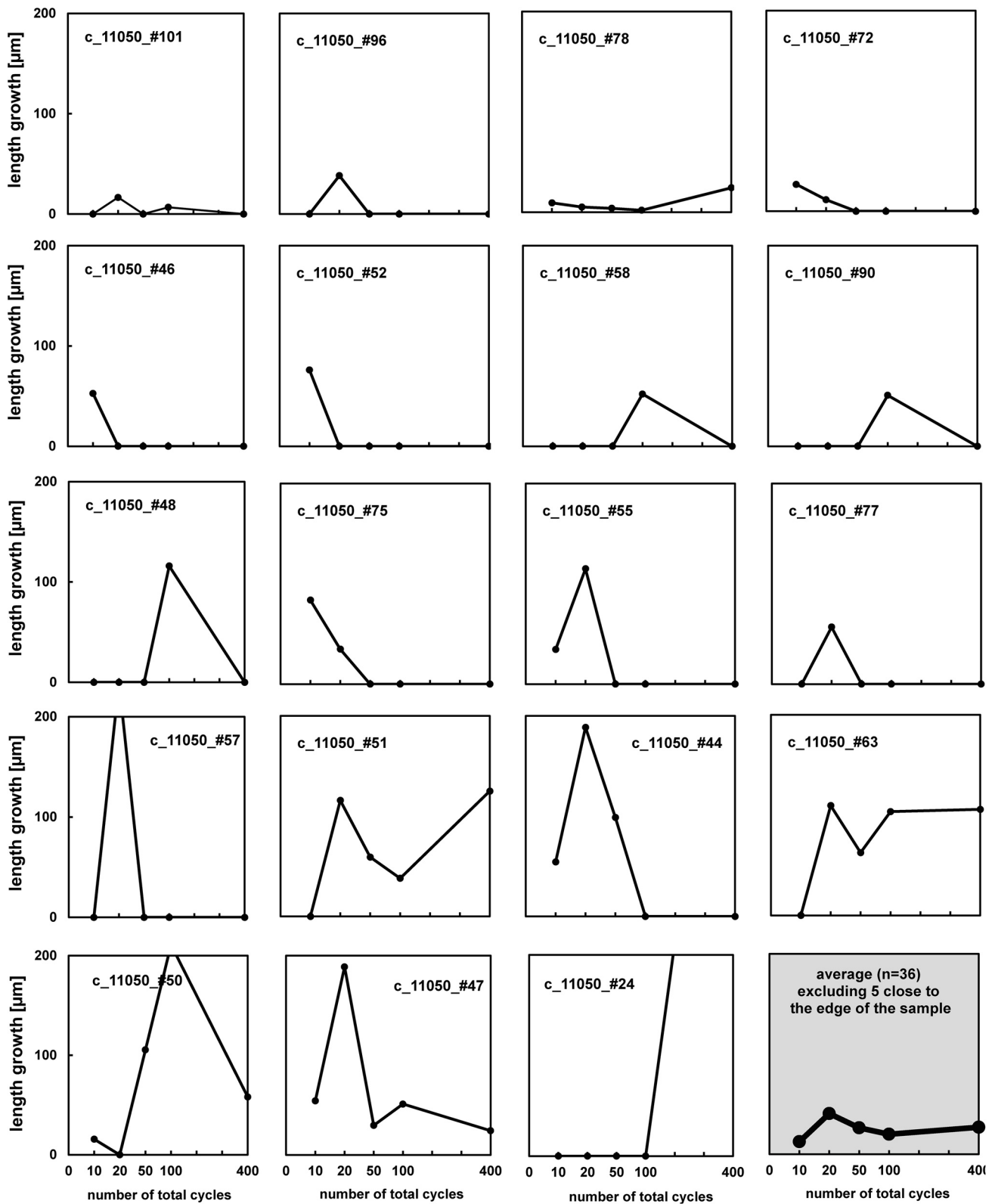


Figure 7. Plot showing the length growth in μm as a function of the total amount of cycles run for selected cracks observed on the surface of the eucrite NWA 11050. The first data point per plot indicates the growth that happened from 0 to 10 cycles, where the second indicates the growth that happened from 11 to 20 cycles, and so on. Note that most of the growths are below 200 μm , except for #57 (235 μm), #50 (211 μm), and #24 (636 μm).

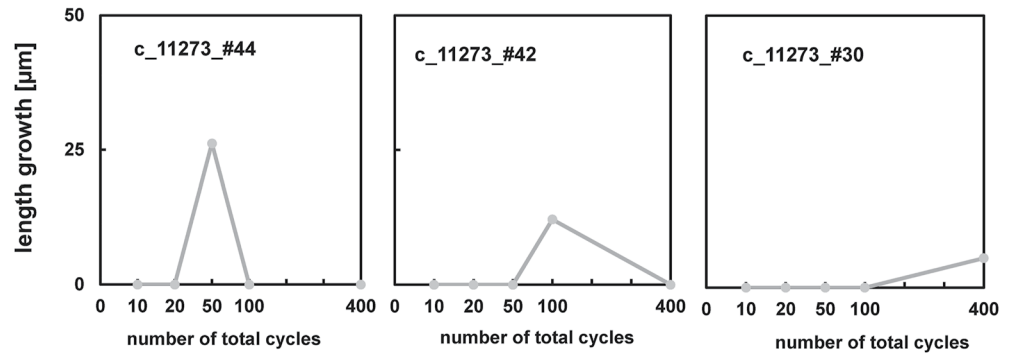


Figure 8. Plot showing the length growth in μm as a function of the total amount of cycles run for selected cracks observed on the surface of the lunar anorthosite breccia NWA 11273. The first data point per plot indicates the growth that happened from 0 to 10 cycles, where the second indicates the growth that happened from 11 to 20 cycles, and so on. Note, that the scale for the length growth is only 1/4 to that of Figure 7.

containing common impact glasses are contributing to a fine-grained, tenth-of- μm -sized, soil as soon as they are exposed to diurnal temperature variations on the surface of the Moon or NEA.

5.2. Lower Cracking Rates Compared to Previous Work

Crack formation and extension rate on the surface of both samples is clearly below that previously reported for Murchison (CM) and Sahara 97210 (OC) by a similar experimental setup, although carried out in nitrogen atmosphere at 1 bar Delbo et al. (2014) showed that the cracks in the studied ordinary chondrite are shorter and their volume smaller, when compared to those of the measured CM chondrite. However, the reported crack length growths for a similar number of cycles (~ 400) is up to 250 μm for the CM and up to ~ 80 μm at maximum. We found maximum crack length growths of up to 26 μm for the lunar anorthosite and up to 636 μm for the eucrite NWA 11050, respectively. The average growth rate for NWA 11050, however, is only ~ 36 $\mu\text{m}/400$ cycles and there seems to be no clear trend for a growth pattern (i.e., exponential or linear) for increasing number of cycles applied (Figure 7). One crack growth (235 μm ; c_11050_#57) happened after 20c, whereas no change was detected after the first 10 cycles and after 50c, 100c, and 400c. For other cracks, the growth rate increased first and decreased afterward (e.g., c_11050_#50, c_11050_#47, or c_11050_#75; Figure 7). Growth rate of cracks in the lunar anorthosite breccia NWA 11273 is clearly below that of the eucrite NWA 11050 and is about 3 $\mu\text{m}/400$ cycles (e.g., Figure 8). As shown in Figure 8, this growth rate is, however, not based on many data as there are less cracks detected when compared to the eucrite NWA 11050 and, additionally, these cracks are leading to micro-flaking in many cases as discussed before. Based on the data presented by Delbo et al. (2014), crack growth in the CM chondrite Murchison as well as in the ordinary chondrite Sahara 97210 seems to be in general positive (i.e., is higher after 400 cycles relative to that after 70 cycles). This is in contrast to the general trend as well as in the absolute growth rates for the basaltic eucrite NWA 11050 (Figure 7) and especially for the lunar anorthosite NWA 11273 (Figure 8). This finding might be attributed to either one or a combination of the following effects:

1. Differences in the mineralogy and therefore strength of the rock; that is, Murchison being a water-bearing, phyllosilicate-rich chondritic rock and Sahara 97210 being a chondritic rock (L/LL3.2). Both are quite different from the rocks studied here.
2. Cycling under high vacuum reduced the heat transport to be solely controlled by conduction rather than by convection. This would be more similar to natural conditions on atmosphere-free surfaces.
3. Adsorbed water molecules that were not removed by the N atmosphere enhanced crack formation by lowering the strength of the rocks (i.e., Eppes & Keanini, 2017; Orowan, 1944) and increase the crack propagation (e.g., Atkinson, 1979; Dunning, 1978; Waza et al., 1980).
4. The use of N atmosphere, which possibly acts in similar ways as water, although in lesser extent.
5. Differences in the degree of terrestrial weathering, that is, the amount of iron hydroxides that result from the oxidation of FeNi metal while the meteorite is exposed to Earth' atmosphere. Since these iron hydroxides have a larger volume compared to the FeNi metal, their formation could potentially introduce stresses and artificial cracks. Additionally, dissolved Fe from the metal is redeposited by aqueous fluid into voids and pre-existing

cracks as Fe-hydroxides increasing the thermal conductivity of the sample. Internal tests (Text S1, Figure S1 in Supporting Information S1) have shown how Fe-hydroxides are reacting already after a few cycles with the formation of cracks. Therefore, the samples used in this study are investigated previously to verify the lowest possible alteration.

The overall lower crack growth rate for lunar anorthosite NWA 11723 and eucrite NWA 11050 (Figures 7 and 8) has implications for airless silicate planetary bodies, that is, the Moon: The primary mineralogy of the rocks exposed to space influences how fast cracks grow and form and need to be considered when investigating more recent (i.e., basaltic) or highly mature and consolidated regolith breccias. At least for the here studied rock types, the time scales that are required to fragment a rock of a given size might be longer than previously described (Delbo et al., 2014): the crack growth rate for the eucrite sample studied here is only ~50% (~0.2 vs. 0.43 mm/yr) of the samples studied in Delbo et al. (2014). However, it needs to be stated, that Molaro et al. (2017) question the breakdown rates modeled by Delbo et al. (2014). The thermal fatigue lifetime of a sample covers different regimes including crack initiation, stable crack growth, and unstable crack growth. The applied model in Delbo et al. (2014) and similar works refer to the Paris law, which can only be applied to the stable crack growth-phase. Since Delbo et al. (2014) constrain the breakdown rate in their model by using initial crack lengths of 30 μm which are in the regime of crack initiation, for which the Paris law cannot be applied. Thus, the breakdown rates calculated by Delbo et al. (2014) are too high (Molaro et al., 2017). Nonetheless, also for lunar anorthosite breccias and basaltic eucrites, thermal fatigue is a relevant process for the formation of regolith on the surface of planetary bodies as seen by the formation of cracks under the here used conditions. In case of the Moon, different responses between areas dominated by consolidated regolith and basalt plains should be expected due to their mineralogic and petrologic differences. Although no lunar basalt has been experimentally cycled, the eucrite (with being a basalt) is mineralogically similar to lunar basalts. The difference in crack formation rate between the lunar anorthosite and the eucrite is very likely controlled by its mineralogy and internal structure clarifying the question of which petrologic context favors cracks development.

5.3. Petrologic Context of Crack Formation

Cracks in the eucrite NWA 11050 are observed to occur between different components close to or on grain boundaries. These stresses occurring on the interfaces between different minerals have been addressed by Molaro et al. (2015). They state that different thermal expansion coefficients, different Young modulus of the adjacent constituents and their modal abundance influence the average stresses. These stresses can be amplified at the tip of pore spaces and at surface-parallel boundaries of the constituents. Most rocks we observe today in our meteorite collections are more or less complex assemblages of quite different minerals with different crystallographic and therefore physical properties (e.g., Weisberg et al., 2006). This includes typical cleavages but also the thermal conductivity of these minerals and how the petrologic context and type of the rock (e.g., Consolmagno et al., 2008; Flynn et al., 2018; Macke et al., 2011; Opeil et al., 2010; Weisberg et al., 2006). Usually, rocks such as basalts (eucrites) or gabbros, that is, typical rocks produced on differentiated planetary bodies, consist of individual crystals. Other rocks such as chondrites of different types, which originate from smaller undifferentiated asteroids, are assemblages of different constituents that formed in different processes, at different times, and under different conditions and were later accreted (e.g., Wasson, 1985; Weisberg et al., 2006). These constituents include chondrules (once molten droplets consisting of olivine, pyroxene, and mesostasis), metal and sulfide grains, and fine-grained matrix (e.g., Connolly & Jones, 2016; Rubin & Ma, 2021; Scott & Krot, 2003). Considering this, a first order assumption would be, that a chondritic rock that is exposed to diurnal temperature variation on the surface of an asteroids would crack along the weakest parts of the, that is, along “constituent boundaries”: Instead of cracking an intact chondrule, the crack would form around the chondrule through the fine-grained matrix separating the constituents from each other if no other planes of relative weakness such as shock planes exist. Hazeli et al. (2018) studied the L6 chondrite Grosvenor Mountains 85209 and cycled it from 28 to 200°C (under atmosphere). They found two major consequences of their experiment on the studied chondrite: (a) Fragments formed from this chondrite by thermal fatigue tend to be rounded, because the phases and microstructure involved have a rounded character. (b) The resulting regolith will be “mainly monomineralic,” because the interfaces between the components are determining, where the rock will crack. However, we note that the term monomineralic might be misleading in this case, since Hazeli et al. (2018) argue that cracks develop along chondrules, which are essentially a constituent consisting of different minerals. Nonetheless, they were able to show that the response of a chondritic rock to thermal fatigue relies heavily on the internal structure of this rock. Follow-up studied by

Liang et al. (2020) extended the approach from Hazeli et al. (2018) by constraining the stress fields for the same meteorite sample. They conclude that the distribution of stress within the sample will more likely be damaged by “interfacial debonding” when subjected to thermal cycling (Liang et al., 2020). Following the implications of Hazeli et al. (2018) and Liang et al. (2020) the regolith produced by thermal fatigue resulting from the eucrite is likely consisting of angular minerals rather than rounded components as for chondrites.

Shock metamorphism of meteorites introduces weak zones into any type of rock: Even at low shock stages, planar fractures can be observed in olivine grains in for example, ordinary chondrites (e.g., Stöffler et al., 2018). High-velocity impacts are a common process and therefore also shock effects in minerals should be the rule as shown for a majority of ordinary chondrites (Bischoff et al., 2019; Stöffler et al., 1988, 2018). This influences the implications from the previous paragraph: Pre-existing cracks and/or weakened zones in minerals due to impacts in a rock might act as nuclei for extending cracks (Molaro, Hergenrother et al., 2020), which would fasten the comminution of these rocks.

Our observation on the petrologic context of crack formation and the findings of Molaro et al. (2015), Hazeli et al. (2018), and Liang et al. (2020) support the relevance of the internal (micro)structure of rocks for the resulting regolith that forms by thermal fatigue.

5.4. Concluding Remarks and Implications for Rock Breakdown and Soil Formation

We performed thermal cycling of a lunar anorthosite breccia and a basaltic eucrite between 200 and 375 K simulating the diurnal temperature variations typically observed for the Moon under realistic high vacuum conditions. Using a cryostat allowed to avoid unrealistic maximum temperatures to cover the expected ΔT . Micro-flaking—the formation and detachment of tenth-of- μm -sized particles on the surface—are observed on both samples, but are 5 \times more abundant on the lunar anorthositic breccia NWA 11273. Formation and growth of cracks has been more often observed on the eucrite NWA 11050. This implies that the type of rock and its mineralogy is of fundamental importance for the type of fragments and soil, which forms through the effects of thermal breakdown certainly including thermal fatigue. While solid rocks with a coherent structural integrity such as magmatic or possibly also metamorphic rocks react to thermal fatigue with the formation of cracks as shown by the basaltic eucrite NWA 11050, rocks which are highly reworked in the regolith of planetary bodies (i.e., the Moon) and are of higher maturity such as the lunar anorthositic breccia NWA 11273, contribute to fine-grained, tenth-of- μm -sized soil as shown by the micro-flaking observed on the sample. This agrees with observations of the size-frequency distribution of lunar soil (e.g., Warren & Korotev, 2022). Additionally, the specific mineralogy of exposed rocks and how easy it is to comminute them by impacts and introduce planes of relative weaknesses (such as cleavages of plagioclase and pyroxene and mosaicism in olivine) by excavating them can also affect the rate of decomposition by thermal fatigue.

However, compared to the durations of rock breakdown experimentally shown and modeled by Delbo et al. (2014) for an ordinary and carbonaceous chondrite, the rates determined in this experiment seem to be dramatically lower for lunar anorthosites and slightly lower for basaltic eucrites. However, it has been shown, that the breakdown rates calculated by Delbo et al. (2014) are overestimated by inaccurate application of the Paris law to their observations (e.g., Molaro et al., 2017). That no crack growth was found in 3D μCT scans excludes that cracks with widths $>\sim 16 \mu\text{m}$ developed in the interior of the samples. Since this experiment is likely able to reproduce thermal fatigue on the grain scale, the results emphasize that thermal fatigue caused by diurnal temperature variations is of importance for the breakdown of rocks and the formation of a regolith on airless bodies, but highly depends on the mineralogy of the rocks that are exposed to these variations. The here investigated processes act at the scale of the diurnal thermal skin depth and thus these implications concern only small cm-scale rocks or the surficial layer of larger rocks. The overall lower cracking rate might well be due to more natural experimental conditions, that is, high vacuum conditions that reduce the thermal conductivity of the experiment to be solely controlled by grain-grain boundaries and the cement between grains. Although the thermal gradient of $\sim 2 \text{ K/min}$ was used, it is noteworthy to mention that this value does not qualify as threshold to separate the effects of thermal fatigue and thermal shock as clearly shown by Molaro et al. (2015), but was rather selected to maintain comparability to previous studies.

In light of these results, shattering by meteoroids ($> \sim 1$ mm) and abrasion by micrometeoroid ($< \sim 1$ mm) bombardment, the major agents of lunar rock erosion, might work in conjunction with thermal fatigue in the case of rocks petrologically susceptible to thermal stresses.

Data Availability Statement

The data used for interpreting the crack growth and micro-flake formation in this study are available under <https://doi.org/10.26022/IEDA/112505> (Patzek & Rüsçh, 2022).

References

- Atkinson, B. K. (1979). A fracture mechanics study of subcritical tensile cracking of quartz in wet environments. *Pure and Applied Geophysics*, 117(5), 1011–1024. <https://doi.org/10.1007/bf00876082>
- Atkinson, B. K. (1984). Subcritical crack growth in geological materials. *Journal of Geophysical Research*, 89(B6), 4077–4114. <https://doi.org/10.1029/JB089iB06p04077>
- Bandfield, J. L., Ghent, R. R., Vasavada, A. R., Paige, D. A., Lawrence, S. J., & Robinson, M. S. (2011). Lunar surface rock abundance and regolith fines temperatures derived from LRO Diviner Radiometer data. *Journal of Geophysical Research*, 116, E00H02. <https://doi.org/10.1029/2011je003866>
- Barghouty, A. F., Meyer, F. W., Harris, P. R., & Adams, J. H., Jr. (2011). Solar-wind protons and heavy ions sputtering of lunar surface materials. *Nuclear Instruments and Methods in Physics Research Section B: Beam Interactions with Materials and Atoms*, 269(11), 1310–1315. <https://doi.org/10.1016/j.nimb.2010.12.033>
- Bischoff, A., Schleitinger, M., & Patzek, M. (2019). Shock stage distribution of 2280 ordinary chondrites—Can bulk chondrites with a shock stage of S6 exist as individual rocks? *Meteoritics & Planetary Sciences*, 54(10), 2189–2202. <https://doi.org/10.1111/maps.13208>
- Bischoff, A., Schleitinger, M., Wieler, R., & Patzek, M. (2018). Brecciation among 2280 ordinary chondrites—Constraints on the evolution of their parent bodies. *Geochimica et Cosmochimica Acta*, 238, 516–541. <https://doi.org/10.1016/j.gca.2018.07.020>
- Bischoff, A., Scott, E. R., Metzler, K., & Goodrich, C. A. (2006). Nature and origins of meteoritic breccias. In *Meteorites and the early solar system II* (pp. 679–712).
- Boelhouwers, J., & Jonsson, M. (2013). Critical assessment of the $2^{\circ}\text{C}\cdot\text{min}^{-1}$ threshold for thermal stress weathering. *Geografiska Annaler - Series A: Physical Geography*, 95(4), 285–293. <https://doi.org/10.1111/geoa.12026>
- Cambioni, S., Delbo, M., Poggiali, G., Avdellidou, C., Ryan, A. J., Deshapriya, J. D. P., et al. (2021). Fine-regolith production on asteroids controlled by rock porosity. *Nature*, 598(7879), 49–52. <https://doi.org/10.1038/s41586-021-03816-5>
- Carrier, W. D. (1973). Lunar soil grain size distribution. *The Moon*, 6(3), 250–263. <https://doi.org/10.1007/bf00562206>
- Cintala, M. J., & Hoerz, F. (1992). An experimental evaluation of mineral-specific comminution. *Meteoritics*, 27(4), 395–403. <https://doi.org/10.1111/j.1945-5100.1992.tb00221.x>
- Connolly, H. C., Jr., & Jones, R. H. (2016). Chondrules: The canonical and noncanonical views. *Journal of Geophysical Research: Planets*, 121, 1885–1899. <https://doi.org/10.1002/2016je005113>
- Consolmagno, G. J., Britt, D. T., & Macke, R. J. (2008). The significance of meteorite density and porosity. *Geochemistry*, 68(1), 1–29. <https://doi.org/10.1016/j.chemer.2008.01.003>
- Crozaz, G., Walker, R., & Woolum, D. (1971). Nuclear track studies of dynamic surface processes on the moon and the constancy of solar activity. In *Proceedings of the lunar science conference* (Vol. 3, pp. 2543–2558).
- Delbo, M., Libourel, G., Wilkerson, J., Murdoch, N., Michel, P., Ramesh, K. T., et al. (2014). Thermal fatigue as the origin of regolith on small asteroids. *Nature*, 508(7495), 233–236. <https://doi.org/10.1038/nature13153>
- Dunning, J. D. (1978). A microscopic, submicroscopic, and microseismic analysis of stable crack propagation and the effect of chemical environment on stable crack propagation in synthetic quartz (Ph. D. Thesis.).
- Eppes, M. C., & Keanini, R. (2017). Mechanical weathering and rock erosion by climate-dependent subcritical cracking. *Reviews of Geophysics*, 55(2), 470–508. <https://doi.org/10.1002/2017rg000557>
- Flynn, G. J., Consolmagno, G. J., Brown, P., & Macke, R. J. (2018). Physical properties of the stone meteorites: Implications for the properties of their parent bodies. *Geochemistry*, 78(3), 269–298. <https://doi.org/10.1016/j.chemer.2017.04.002>
- Hartung, J. B., Hörz, F., & Gault, D. E. (1972). Lunar microcraters and interplanetary dust. In *Lunar and planetary science conference proceedings* (Vol. 3, p. 2735).
- Hazeli, K., El Mir, C., Papanikolaou, S., Delbo, M., & Ramesh, K. T. (2018). The origins of asteroidal rock disaggregation: Interplay of thermal fatigue and microstructure. *Icarus*, 304, 172–182. <https://doi.org/10.1016/j.icarus.2017.12.035>
- Hörz, F., Basilevsky, A. T., Head, J. W., & Cintala, M. J. (2020). Erosion of lunar surface rocks by impact processes: A synthesis. *Planetary and Space Science*, 194, 105105. <https://doi.org/10.1016/j.pss.2020.105105>
- Horz, F., & Cintala, M. (1997). Impact experiments related to the evolution of planetary regolith. *Meteoritics & Planetary Sciences*, 32(2), 179–209. <https://doi.org/10.1111/j.1945-5100.1997.tb01259.x>
- Hörz, F., Cintala, M. J., See, T. H., Cardenas, F., & Thompson, T. D. (1984). Grain size evolution and fractionation trends in an experimental regolith. *Journal of Geophysical Research*, 89(S01), C183–C196. <https://doi.org/10.1029/jb089is01p0c183>
- Hörz, F., Hartung, J. B., & Gault, D. E. (1971). Micrometeorite craters on lunar rock surfaces. *Journal of Geophysical Research*, 76(23), 5770–5798. <https://doi.org/10.1029/jb076i023p05770>
- Horz, F., Schneider, E., & Hill, R. E. (1974). Micrometeoroid abrasion of lunar rocks: A Monte Carlo simulation. In *Lunar and planetary science conference proceedings* (Vol. 3, pp. 2397–2412).
- Housley, R. M., Cirlin, E. H., Paton, N. E., & Goldberg, I. B. (1974). Solar wind and micrometeorite alteration of the lunar regolith. In *Lunar and planetary science conference proceedings* (Vol. 5, pp. 2623–2642).
- Jiang, S., Tang, C., Li, X., Tan, Y., Peng, R., Yang, D., & Liu, S. (2020). Discrete element modeling of the machining processes of brittle materials: Recent development and future perspective. *International Journal of Advanced Manufacturing Technology*, 109(9), 2795–2829. <https://doi.org/10.1007/s00170-020-05792-y>
- Keil, K. (1982). Composition and origin of chondritic breccias. In *Lunar breccias and soils and their meteoritic analogs* (p. 65).

Acknowledgments

M.P and O.R are supported by a Sofja Kovalevskaja Award Project of the Alexander von Humboldt Foundation. Reiner Zielke and Christian Bussmann (TU Dortmund) are thanked for μCT scans of the studied samples. Philip Maus is thanked for initial data reduction. Ulla Heitmann is thanked for sample preparation. R. Schmidt is thanked for technical assistant on the cryostat. The authors thank J. Molaro, an anonymous reviewer, and the associate editor D. Rogers for their comments and suggestions that helped to improve this manuscript. Open Access FUNDING enabled and organized by Projekt DEAL.

- Klein, C., Hurlbut, C. S., & Dana, J. D. (1985). *Manual of mineralogy: (After James D. Dana)*. Wiley.
- Krokosky, E. M., & Husak, A. (1968). Strength characteristics of basalt rock in ultra-high vacuum. *Journal of Geophysical Research*, 73(6), 2237–2247. <https://doi.org/10.1029/JB073i006p02237>
- Lee, M. R., & Bland, P. A. (2004). Mechanisms of weathering of meteorites recovered from hot and cold deserts and the formation of phyllosilicates. *Geochimica et Cosmochimica Acta*, 68(4), 893–916. [https://doi.org/10.1016/s0016-7037\(03\)00486-1](https://doi.org/10.1016/s0016-7037(03)00486-1)
- Levi, F. A. (1976). Thermal deformation and fracturing in olivine-rich samples. *Meteoritics*, 11(2), 101–109. <https://doi.org/10.1111/j.1945-5100.1976.tb00157.x>
- Liang, B., Cuadra, J., Hazeli, K., & Soghrati, S. (2020). Stress field analysis in a stony meteorite under thermal fatigue and mechanical loadings. *Icarus*, 335, 113381. <https://doi.org/10.1016/j.icarus.2019.07.015>
- Libourel, G., Ganino, C., Delbo, M., Niezgodza, M., Rémy, B., Aranda, L., & Michel, P. (2021). Network of thermal cracks in meteorites due to temperature variations: New experimental evidence and implications for asteroid surfaces. *Monthly Notices of the Royal Astronomical Society*, 500(2), 1905–1920. <https://doi.org/10.1093/mnras/staa3183>
- Liu, S. F., Lu, S. F., Wan, Z. J., & Cheng, J. Y. (2019). Investigation of the influence mechanism of rock damage on rock fragmentation and cutting performance by the discrete element method. *Royal Society Open Science*, 6(5), 190116. <https://doi.org/10.1098/rsos.190116>
- Macke, R. J., Consolmagno, G. J., & Britt, D. T. (2011). Density, porosity, and magnetic susceptibility of carbonaceous chondrites. *Meteoritics & Planetary Sciences*, 46(12), 1842–1862. <https://doi.org/10.1111/j.1945-5100.2011.01298.x>
- MacLennan, E. M., & Emery, J. P. (2022). Thermophysical investigation of asteroid surfaces. II. Factors influencing grain size. *The Planetary Science Journal*, 3(2), 47. <https://doi.org/10.3847/psj/ac4967>
- Molaro, J., & Byrne, S. (2012). Rates of temperature change of airless landscapes and implications for thermal stress weathering. *Journal of Geophysical Research*, 117, E10011. <https://doi.org/10.1029/2012je004138>
- Molaro, J. L., Byrne, S., & Langer, S. A. (2015). Grain-scale thermoelastic stresses and spatiotemporal temperature gradients on airless bodies, implications for rock breakdown. *Journal of Geophysical Research: Planets*, 120, 255–277. <https://doi.org/10.1002/2014je004729>
- Molaro, J. L., Byrne, S., & Le, J. L. (2017). Thermally induced stresses in boulders on airless body surfaces, and implications for rock breakdown. *Icarus*, 294, 247–261. <https://doi.org/10.1016/j.icarus.2017.03.008>
- Molaro, J. L., Hergenrother, C. W., Chesley, S. R., Walsh, K. J., Hanna, R. D., Haberle, C. W., et al. (2020). Thermal fatigue as a driving mechanism for activity on asteroid Bennu. *Journal of Geophysical Research: Planets*, 125, e2019JE006325. <https://doi.org/10.1029/2019je006325>
- Molaro, J. L., Walsh, K. J., Jawin, E. R., Ballou, R. L., Bennett, C. A., Della Giustina, D. N., et al. (2020). In situ evidence of thermally induced rock breakdown widespread on Bennu's surface. *Nature Communications*, 11(1), 1–11. <https://doi.org/10.1038/s41467-020-16528-7>
- Opeil, C. P., Britt, D. T., Macke, R. J., & Consolmagno, G. J. (2020). The surprising thermal properties of CM carbonaceous chondrites. *Meteoritics & Planetary Sciences*, 55(8), maps.13556. <https://doi.org/10.1111/maps.13556>
- Opeil, C. P., Consolmagno, G. J., & Britt, D. T. (2010). The thermal conductivity of meteorites: New measurements and analysis. *Icarus*, 208(1), 449–454. <https://doi.org/10.1016/j.icarus.2010.01.021>
- Orowan, E. (1944). The fatigue of glass under stress. *Nature*, 154(3906), 341–343. <https://doi.org/10.1038/154341a0>
- Patzek, M., & Rüsçh, O. (2022). *Data set for experimentally induced thermal fatigue on lunar and eucrite meteorites – influence of the mineralogy on rock breakdown, Version 1.0*. Interdisciplinary Earth Data Alliance (IEDA). <https://doi.org/10.26022/IEDA/112505>
- Pieters, C. M., & Noble, S. K. (2016). Space weathering on airless bodies. *Journal of Geophysical Research: Planets*, 121, 1865–1884. <https://doi.org/10.1002/2016JE005128>
- Piqueux, P., & Christensen, P. R. (2009). A model of thermal conductivity for planetary soils: 1. Theory for unconsolidated soils. *Journal of Geophysical Research*, 114, E09006. <https://doi.org/10.1029/2008JE003309>
- Ravaji, B., Alí-Lagoa, V., Delbo, M., & Wilkerson, J. W. (2019). Unraveling the mechanics of thermal stress weathering: Rate-effects, size-effects, and scaling laws. *Journal of Geophysical Research: Planets*, 124, 3304–3328. <https://doi.org/10.1029/2019je006019>
- Richter, D., & Simmons, G. (1974). Thermal expansion behavior of igneous rocks. In *International Journal of Rock Mechanics and Mining Sciences & Geomechanics Abstracts* (Vol. 11(10), pp. 403–411). Pergamon.
- Righter, K., & Drake, M. J. (1997). A magma ocean on Vesta: Core formation and petrogenesis of eucrites and diogenites. *Meteoritics & Planetary Sciences*, 32(6), 929–944. <https://doi.org/10.1111/j.1945-5100.1997.tb01582.x>
- Rubin, A., & Ma, C. (2021). In *Meteorite mineralogy* (Vol. 26). Cambridge University Press.
- Ruesch, O., Sefton-Nash, E., Vago, J. L., Küppers, M., Pasckert, J. H., Krohn, K., & Otto, K. (2020). In situ fragmentation of lunar blocks and implications for impacts and solar-induced thermal stresses. *Icarus*, 336, 113431. <https://doi.org/10.1016/j.icarus.2019.113431>
- Scott, E. R. D., & Krot, A. N. (2003). Chondrites and their components. *Treatise on Geochemistry*, 1, 711.
- Shoemaker, E. M. (1971). Origin of fragmental debris on the lunar surface and the history of bombardment of the moon. In *I Seminario de Geologia Lunar*. University of Barcelona (Rev). Presentation at.
- Stöffler, D., Bischoff, A., Buchwald, V., & Rubin, A. E. (1988). Shock effects in meteorites. *Meteorites and the early solar system* (pp. 165–202). Stöffler, D., Hamann, C., & Metzler, K. (2018). Shock metamorphism of planetary silicate rocks and sediments: Proposal for an updated classification system. *Meteoritics & Planetary Sciences*, 53(1), 5–49. <https://doi.org/10.1111/maps.12912>
- Taylor, L. A., Pieters, C., Patchen, A., Taylor, D. H. S., Morris, R. V., Keller, L. P., & McKay, D. S. (2010). Mineralogical and chemical characterization of lunar highland soils: Insights into the space weathering of soils on airless bodies. *Journal of Geophysical Research*, 115, E02002. <https://doi.org/10.1029/2009je003427>
- Uribe-Suárez, D., Delbo, M., Bouchard, P. O., & Pino-Muñoz, D. (2021). Diurnal temperature variation as the source of the preferential direction of fractures on asteroids: Theoretical model for the case of Bennu. *Icarus*, 360, 114347. <https://doi.org/10.1016/j.icarus.2021.114347>
- Warren, P. H., & Korotev, R. L. (2022). Ground truth constraints and remote sensing of lunar highland crust composition. *Meteoritics & Planetary Sciences*, 57(2), 527–557. <https://doi.org/10.1111/maps.13780>
- Wasson, J. T. (1985). *Meteorites: Their record of early solar-system history*. Freeman.
- Waza, T., Kurita, K., & Mizutani, H. (1980). The effect of water on the subcritical crack growth in silicate rocks. *Tectonophysics*, 67(1–2), 25–34. [https://doi.org/10.1016/0040-1951\(80\)90162-6](https://doi.org/10.1016/0040-1951(80)90162-6)
- Weisberg, M. K., McCoy, T. J., & Krot, A. N. (2006). Systematics and evaluation of meteorite classification. In *Meteorites and the early solar system II* (Vol. 19, pp. 19–52). <https://doi.org/10.2307/j.ctv1v7zdm8>
- Zeng, X., Li, S., Joy, K. H., Li, X., Liu, J., Li, Y., et al. (2020). Occurrence and implications of secondary olivine veinlets in lunar highland breccia Northwest Africa 11273. *Meteoritics & Planetary Sciences*, 55(1), 36–55. <https://doi.org/10.1111/maps.13421>